DOE GRANT # DE FG 02-05ER84300

HIGH EFFICIENCY, LOW COST SCINTILLATORS FOR PET

FINAL REPORT

March 6, 2007

Kanai Shah, PI

E. PHASE I FINAL REPORT

The research in the Phase I project was designed to establish the feasibility of cerium-doped hafnate compounds, $BaHfO_3$:Ce and $SrHfO_3$:Ce, as ceramic scintillators for PET imaging. The first part of the Phase I research dealt with the synthesis of cerium-doped powders of the selected hafnate compounds and measurement of their diffraction pattern and scintillation properties, including light yield, emission spectra, and decay time. Then, using the suitable synthesized powders, optical ceramics of $BaHfO_3$:Ce and $SrHfO_3$:Ce were fabricated and their physical and scintillation properties were characterized. Finally, 511 keV gamma ray energy and timing spectra were collected using selected samples. Overall, the Phase I research was very successful and we were able to clearly demonstrate the feasibility of the proposed approach.

1. POWDER PREPARATION AND EVALUATION

a. Synthesis of Cerium Doped $SrHfO_3$ and $BaHfO_3$

Although a lower temperature flux technique has been reported in the literature [i], we found the simplest and most reliable synthesis procedure to be high-temperature solid-state reaction between the respective binary oxides. For example, the first step in making $BaHfO_3$:Ce was to mix the oxides of barium and hafnium (BaO and HfO_2) in a 1:1 molar ratio with regard to the metal ion. This mixed powder was then transferred to a zirconia cup of a ball mill (Fritsch, Pulverisette#7) in the form of an acetone slurry, to which a solution of cerium aluminate was added in the appropriate amount to achieve the desired doping level, in the range of 0.05 to 1 mole percent. About 50 zirconia balls (5mm diameter) were placed on top of the powder slurry and the solution was milled for about 5 minutes at slow speed to obtain a thixotropic mixture. If necessary, more acetone was added to insure a thick, running mixture of powders and acetone, followed by milling for at least 3 hours at medium speed. A thick slurry was obtained after milling.

After the slurry was stirred to mix the oxides, acetone was allowed to evaporate at or slightly above room temperature. The resulting mixture was ground to allow intimate mixing of the constituents, and then transferred to the die of a pellet press to create dense powder pellets, which were then heated in argon-hydrogen gas mixture to 1400°C for about 1 hour to drive off the water and aluminates. Next, the pellet was heated in presence of H_2 at 1700°C for about 6 hours to synthesize $BaHfO_3$:Ce. The high temperature assures a sufficiently high diffusion rate to achieve complete chemical reaction and to incorporate cerium into the host lattice, while the use of H_2 keeps Ce in the desired 3+ oxidation state. The synthesis of the $SrHfO_3$:Ce was performed in a similar manner by replacing BaO with SrO in the procedure, at the appropriate 1:1 metal ion ratio. The powders of $SrHfO_3$:Ce and $BaHfO_3$:Ce, prepared in this manner, were then evaluated.

b. X-ray Diffraction Analysis of $BaHfO_3$:Ce and $SrHfO_3$:Ce

Barium hafnate and strontium hafnate powders (doped with Ce^{3+}), synthesized in our study, were analyzed by X-ray diffraction at Massachusetts Institute of Technology (Rigaku Rotaflex #RTP-500). For both hafnate samples, all the observed peaks in the respective diffraction patterns (see **Figure 4**) are consistent with the structures reported in the literature. It should be noted that while $SrHfO_3$ is orthorhombic rather than cubic, its diffraction pattern (top) is remarkably similar to that of its fully cubic barium counterpart (bottom), indicating that the deviation of the former from full cubic symmetry, and the consequent optical anisotropy, are very small. Thus both

materials possess structural properties suitable for fabrication of transparent optical ceramics. The X-ray diffraction results confirm that we have succeeded in synthesizing powders having the requisite structure.

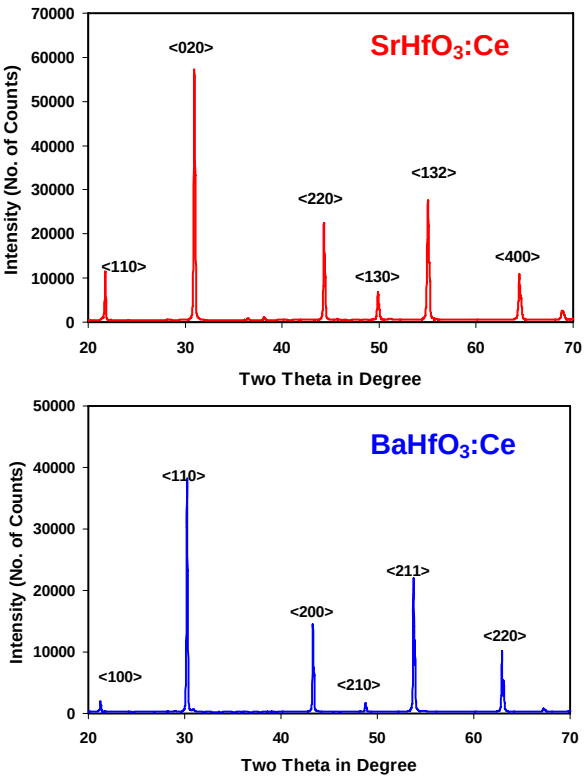

Figure 4. X-ray diffraction pattern of $SrHfO_3$ (top) and $BaHfO_3$ (bottom) powders synthesized at RMD. The diffraction results confirm that the cubic symmetry of $BaHfO_3$ and quasi-cubic (orthorhombic) symmetry of $SrHfO_3$. The structure of $SrHfO_3$ shows minimal deviation

c. Scintillation Properties of $BaHfO_3$:Ce and $SrHfO_3$:Ce

During the Phase I study, we have characterized the luminescence and timing properties of $SrHfO_3$:Ce and $BaHfO_3$:Ce powder samples under X-ray excitation.

i. Luminescence Under X-ray Excitation

The emission spectra of the $SrHfO_3$:Ce and $BaHfO_3$:Ce samples were measured under X-ray irradiation. The specimens were excited with radiation from a Philips X-ray tube having a copper target, with power settings of 30 kV and 15 mA. The scintillation light was passed through a McPherson 0.2-meter monochromator and detected by a Hamamatsu C31034 photomultiplier tube with a quartz window. The system was calibrated with a standard light source to enable correction for sensitivity variations as a function of wavelength. **Figure 5** shows the optical emission spectra of the two hafnate samples. The emission from $SrHfO_3$:Ce hits a maximum at ~410 nm, while that from $BaHfO_3$:Ce peaks at ~400 nm, fully consistent with luminescence due to the $5d \rightarrow 4f$ transition of Ce^{3+}. The presence of such a strong cerium emission provides additional confirmation that we have indeed fabricated the combined oxides, since no significant Ce^{3+} luminescence is observed in any of the starting oxides (SrO, BaO, HfO_2). This result also confirms that the synthesized powders are good enough to serve as the starting materials for ceramic fabrication.

We have also made a comparison of the emission intensity of the pellets prepared from $SrHfO_3$:Ce and $BaHfO_3$:Ce powders with that from a BGO reference sample at the same level of irradiation. Allowing for the differences in geometric shape between the three specimens and the PMT quantum efficiency differences over the wavelength ranges of the respective emissions, we estimate the light output of the $SrHfO_3$:Ce and $BaHfO_3$:Ce pellets to be substantially higher than that of the BGO reference sample. The estimated light output of $SrHfO_3$:Ce is ~45,000

photons/MeV, which is more than five times higher than that for BGO, about two times higher than that of LSO crystals and even slightly higher than NaI:Tl crystals. The light yield of $BaHfO_3$:Ce is estimated to be 28,000 photons/MeV, which is marginally higher than the reported value for high quality LSO single crystals (see **Table 1**). For these early hafnate specimens to have emission higher than that of LSO crystal, a state-of-the-art PET scintillator, is very encouraging and irepresents another favorable portent for our ultimate success.

ii. Timing Characteristics

The temporal behavior of the scintillation from $SrHfO_3$:Ce and $BaHfO_3$:Ce samples was measured using the delayed coincidence method [ii] by Dr. William Moses' group at LBNL (see **Figure 6**). Decay time measurements were made using the LBNL Pulsed X-Ray Facility. The X-ray source is a light-excited X-ray tube that produces 4,000 X-ray photons (mean energy 18.5 keV) per steradian in each 1-ps fwhm pulse, with a 50 kHz repetition rate.

The samples were placed in the X-ray beam and their fluorescent emanations were detected with a sapphire-windowed microchannel plate photomultiplier tube (spectral range 150-650 nm, transit time jitter 40 ps fwhm). The time difference between the X-ray pulse and the detected fluorescent emissions were measured using a TAC/ADC combination having 2 ps fwhm resolution, and the decay time spectra were acquired through the delayed coincidence method [ii]. The total system response time was 60 ps fwhm. The data were then fitted to an exponential decay lifetime model (with multiple decay and rise-times, as needed). The decay curves for $SrHfO_3$:Ce and $BaHfO_3$:Ce samples are shown in **Figure 6**.

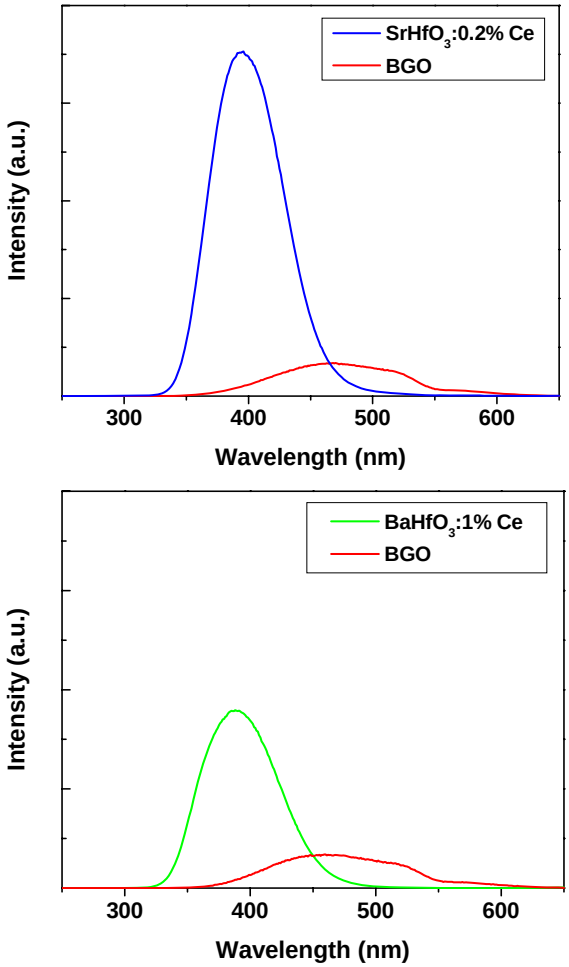

Figure 5. X-ray induced emission spectra for $SrHfO_3$:Ce and $BaHfO_3$:Ce powder samples measured in the Phase I study. Also shown in both plots is the emission spectrum for a reference BGO powder sample

As seen in the figure, the principal decay time constant for both materials is very fast (~16 ns for $BaHfO_3$:Ce and $SrHfO_3$:Ce), as expected for Ce^{3+} luminescence. Even faster principal decay constant (~14 ns) has been recorded for some specimens. The risetime of the scintillation pulses from both materials is also very fast (<0.2 ns). The *initial photon intensity*, a figure of merit for

timing applications, is higher for $BaHfO_3$:Ce and $SrHfO_3$:Ce than for such common inorganic PET scintillators as LSO, BGO and GSO; this indicates that $BaHfO_3$:Ce and $SrHfO_3$:Ce should provide excellent timing resolution and may be suitable for time-of-flight (TOF) PET imaging.

Our results are in good agreement with those reported by Venkataramani [**Error! Bookmark not defined.**]. Overall, these results indicated that the powders we synthesized were indeed of high quality. These powders were then used to fabricate optical ceramic scintillators as discussed in detail in the following section.

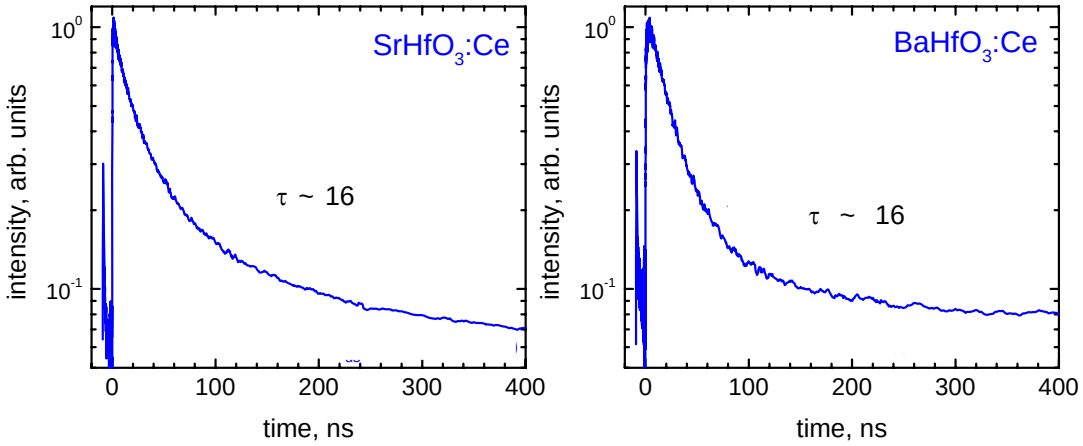

Figure 6. Decay time spectrum for $SrHfO_3$:Ce (left) and $BaHfO_3$:Ce (right) under pulsed X-ray excitation. The principal decay constant was estimated to be ~16 ns, while the rise time was <0.2 ns in

2. Preparation of Ceramic $BaHfO_3$:Ce and $SrHfO_3$:Ce by Hot Pressing

The procedures and experiments described in the previous section confirm that the powders we synthesized in the Phase I research were indeed of high quality. These powders were then used to fabricate optical ceramic scintillators, which involved densification of the powders by controlled application of high temperature and high pressure treatment. To achieve appropriate optical quality, it is important to optimize the powder morphology.

The powder morphology issues are very much dependent on the temperature of synthesis. Ideally, we want particles that are not only chemically pure but also well crystallized, yet small enough to consolidate well with minimal porosity. Here, however, we encounter a conflict: crystallinity is generally much better when synthesis is conducted at higher temperatures, since ion mobility is greater and equilibrium more readily achieved. But when powders are synthesized at high temperatures, a considerable degree of particle growth takes place, and the average particle size increases significantly (up to ~100 μm). This is too large for the successful hot pressing of a highly translucent ceramic. Moreover, many of the particles also sinter together into larger agglomerates, trapping porosity within them. Since the preferred particle size range is 0.1 to 2 μm for the starting powders, we must seek an appropriate balance. Consequently, we explored the feasibility of reducing the particle size and breaking up agglomerates by using a planetary ball mill that is available at RMD (Fritsch, Pulverisette#7). The hafnate powders were placed into a 50-cm^3

zirconium oxide jar, along with 5-mm diameter zirconium oxide grinding balls and methanol. The alkaline-earth hafnate samples were processed at 3200 rpm for 1-3 days. The resulting particle size distributions were analyzed on a Saturn DigiSizer 5200 particle size analyzer and **Figure 7** shows the results for one batch of $BaHfO_3$:Ce, which confirm that after milling the required sub-micron particle size distribution is indeed achieved. Some samples displayed a bimodal distribution of particles, which may improve packing density, although care must be exercised to avoid exaggerated grain growth and the entrapment of porosity, which can act as scattering centers to degrade the translucency. Similar particle size distribution was recorded for $SrHfO_3$:Ce powder after milling. A scanning electron micrograph (SEM) of a cerium doped $BaHfO_3$ powder after milling is shown in **Figure 8** that confirms its sub-micron particle size though some agglomerates are observed.

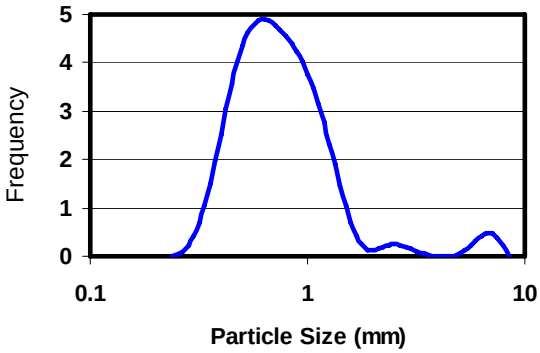

Figure 7. Particle size distribution of milled

These powders were then subjected to high temperature and pressure treatment at Boston University (BU) by Dr. Vinod Sarin's team to create optical ceramics. In addition to powders synthesized in this manner, we also purchased some custom $SrHfO_3$:Ce and $BaHfO_3$:Ce powders with appropriate symmetry (cubic for $BaHfO_3$:Ce and quasi-cubic for $SrHfO_3$:Ce) and sub-micron particle size distribution from Trans-Tech Inc. (Adamstown, MD). The emission spectra and temporal response (under X-ray excitation) for the $SrHfO_3$:Ce and $BaHfO_3$:Ce powders provided by Trans-Tech were very similar to those shown in **Figures 5-6** for same compositions synthesized at RMD. The powders provided by Trans-Tech were also treated at Boston University. We began a study into the actual fabrication of optical ceramic specimens of the two candidate hafnates, and succeeded in producing a number of disks from the powders. The fabrication was accomplished by means of a Centorr vacuum hot press, at a number of settings of the relevant parameters (temperature, pressure, *etc*.) that we chose on the basis of our previous experience with TOC Lu_2O_3:Eu [Lempicki]. The specimens were ~1.5 cm in diameter and ~1-2 mm thick. Ceramic disks of $SrHfO_3$:Ce and $BaHfO_3$:Ce were pressed at three different temperatures (1500°C,

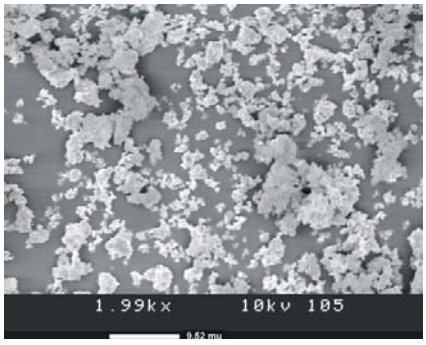

Figure 8. SEM of milled $BaHfO_3$:Ce powder (with 9.52 μm reference bar) confirming sub-μm particle

Figure 9. Photograph of a $BaHfO_3$:Ce ceramic prepared by hot pressing by RMD-ALEM team.

1600°C and 1700°C). The optical quality of both candidates improved substantially at higher temperatures (1600 °C and 1700 °C). **Figure 9** shows a photograph of a ceramic $BaHfO_3$:Ce disk that was pressed after careful adjustment of process parameters, illustrating that optical ceramic hafnate specimens with high degree of transparency were indeed produced in the Phase I effort. This result is very encouraging and bodes well for the overall approach of preparing these promising scintillators using ceramic processing.

X-ray diffraction analysis of the $SrHfO_3$:Ce and $BaHfO_3$:Ce ceramics has been conducted at Boston University. **Figure 10** shows the XRD patterns recorded for $BaHfO_3$:Ce powder as well as for optical ceramics processed from such powders at three different temperatures and results confirmed that the ceramics show the same diffraction pattern, characteristic of cubic crystal structure of $BaHfO_3$, as the precursor powder. The diffraction results for $SrHfO_3$:Ce confirmed that the starting powder as well as processed ceramics had the same quasi-cubic (orthogonal)

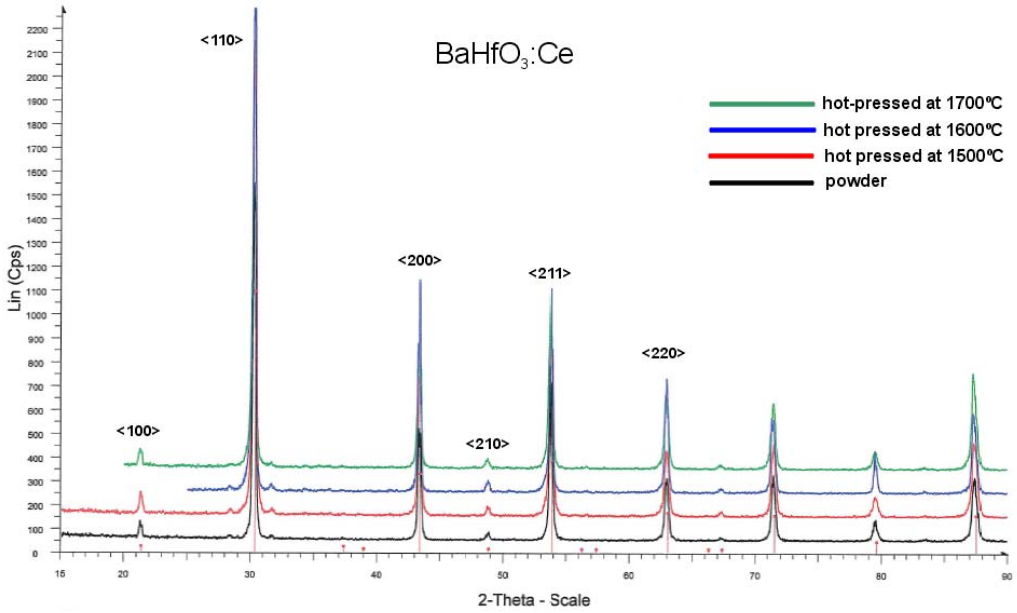

Figure 10. X-ray diffraction patterns for $BaHfO_3$:Ce powder as well as optical ceramics fabricated using hot-pressing at three different temperatures.

crystal symmetry. Overall, the X-ray diffraction and optical quality results are very encouraging and they confirm that we have indeed succeeded in producing optical ceramics of the hafnate compositions using hot-pressing that have the required crystal symmetry and high degree of optical translucency.

Polished ceramic samples were also examined metallographically, optically and by microprobe analysis. A small percentage of second phase was identified in some samples as free HfO_2. The powder was adjusted chemically to bring it to stoichiometry, and subsequent pressings were nearly free of this second phase. It is crucial in the field of optical ceramics that

phase purity be maintained throughout the process. Not only porosity, but second phases act as light scattering centers.

Comment [CB1]: Bill Rhodes to write this?

3. Optical Ceramic Fabrication Using Sintering and Hot Isostatic Pressing (HIP)

In addition to hot-pressing approach (discussed in the previous section), we have also explored an alternative approach for optical ceramic fabrication in collaboration with Dr. Venkatramani at General Electric's Global Research Center (Niskayuna, NY). In this approach, in place of hot-pressing, we used sintering of $SrHfO_3$:Ce powder followed by hot-isostatic pressing (HIP) to create optical ceramic specimens. Using the high quality $SrHfO_3$:Ce powder, pellets was formed at room temperature by mechanical pressing. The pellets were then processed using a cold isostatic press and then presintered in vacuum at ~1700°C. At this point, the processed ceramic had density that is ~93% of that for a single crystal. The specimens were then processed using a hot-isostatic press with temperature ranging from 1700 to 1900 °C and pressure of ~25,000 psi. **Figure 11** shows a photograph of an optical ceramic $SrHfO_3$:Ce sample prepared in this manner. The diameter of the sample is 10 mm and its thickness is ~2 mm and it exhibits good transparency. The typical grain size in such samples is in 10-70 μm range.

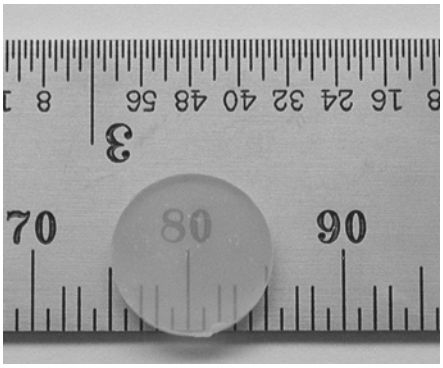

Figure 11. Photograph of optical ceramic $SrHfO_3$:Ce specimen (1 cm diameter, 2 mm thick) fabricated by sinter-HIP processing.

Figure 12 shows an X-ray diffraction pattern of an optical ceramic $SrHfO_3$:Ce specimen fabricated by sinter-HIP processing that confirms that the sample has single phase with the expected quasi-cubic (orthorhombic) symmetry.

4. Optical and Scintillation Properties: Emission, Decay, Transmission, Spectroscopy

Once the optical ceramic $SrHfO_3$:Ce and $BaHfO_3$:Ce specimens were available, we measured their scintillation properties such as decay and emission spectra under X-ray and gamma-ray excitation. The results were compared with those measured earlier for powder specimens of each composition. The effect of cerium concentration on scintillation properties of these hafnates was also evaluated.

Deleted: **Figure 11**. Photograph of an optical ceramic $SrHfO_3$:Ce specimen (1 cm diameter, 2 mm thick) fabricated using sinter-HIP processing.

a. Decay Time Behavior

During the Phase I effort, we evaluated the temporal response of $SrHfO_3$:Ce and $BaHfO_3$:Ce optical ceramic specimens under γ-ray excitation (511 keV photons, ^{22}Na source) using the delayed coincidence method [ii]. The measured temporal responses of $BaHfO_3$:Ce and $SrHfO_3$:Ce ceramic specimens are shown in **Figure 13**. Based on a multi-exponential fit to the data, the risetime was estimated to be <0.2 ns, while the principal decay time constant was estimated to be ~14 ns for a $SrHfO_3$ sample. It should be noted that for $SrHfO_3$:Ce specimens fabricated using hot-pressing as well as sintering-hot isostatic pressing approaches, the decay time behavior was very similar and the principal decay time constant was ~16 ns in both cases. Ce^{3+} concentration was varied over a wide range (0.05% to 1%) in $SrHfO_3$:Ce specimens and the decay time constants were found to be similar across this Ce^{3+} concentration range. From the temporal response of $BaHfO_3$:Ce ceramic specimen shown in **Figure 13**, the principal decay time constant was measured to be ~15 ns along. The risetime was measured to be <0.2 ns. As with $SrHfO_3$:Ce, Ce^{3+} concentration was varied over a wide range (0.05% to 1%) in $BaHfO_3$:Ce specimens and the principal decay time constant was found to be similar across this Ce^{3+} concentration range. A second decay component with 220 ns time constant was also present in some $SrHfO_3$:Ce and BaHfO3:Ce samples (based on the multi-exponential fit to the data).

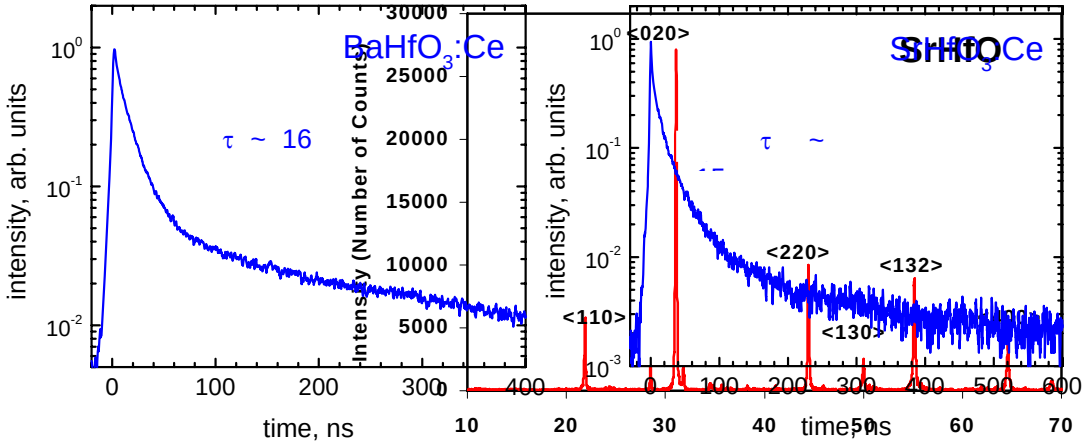

Figure 13. Decay time spectra for $BaHfO_3$:Ce and $SrHfO_3$:Ce ceramic

Figure 12. X-ray diffraction pattern of $SrHfO_3$:Ce ceramic fabricated using sinter-HIP processing.

Overall, the decay time results for $SrHfO_3$:Ce and $BaHfO_3$:Ce ceramics (shown in **Figure 13**) are similar to those discussed earlier for $SrHfO_3$:Ce and $BaHfO_3$:Ce powders (shown in **Figure 6**).

b. Emission Behavior

Emission spectra for $SrHfO_3$:Ce and $BaHfO_3$:Ce ceramic samples under X-ray excitation have been measured in the Phase I project and the results were found to be very similar to those shown in **Figure 5** for powder specimens. The peak emission wavelength for $SrHfO_3$:Ce and $BaHfO_3$:Ce ceramics were measured to be 410 nm and 400 nm, respectively and the emission intensity results for the ceramics also followed the same trends observed earlier with the powder samples.

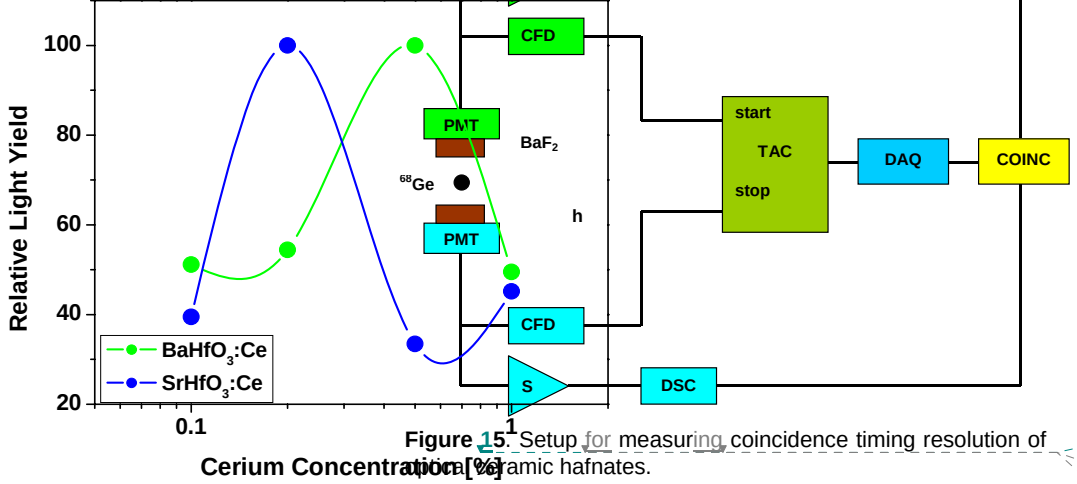

Figure 14. Relative light yield versus Ce^{3+} concentration (on molar basis) for $SrHfO_3$:Ce and $BaHfO_3$:Ce ceramic hafnates.

We have also characterized the effect of cerium concentration on emission intensity of $SrHfO_3$ and $BaHfO_3$ and the results are presented in **Figure 14**. As seen in the figure, the light yield of $SrHfO_3$:Ce peaks at ~0.2 % Ce^{3+} concentration (on molar basis) and drops at higher as well as lower Ce^{3+} concentrations, while that for $BaHfO_3$:Ce peaks at 0.5% Ce^{3+} molar concentration. Thus, we used 0.2 to 0.3% Ce^{3+} concentration for $SrHfO_3$:Ce in later runs to maximize its light yield, while for $BaHfO_3$:Ce we used Ce^{3+} concentration of 0.5% in later runs.

5. GAMMA-RAY STUDIES USING 511 keV PHOTONS

The final set of experiments performed in the Phase I project involved gamma-ray spectroscopy with optical ceramic hafnate specimens. These studies, which included timing and resolution measurements, were conducted only with $SrHfO_3$:Ce ceramics (~1 cm diameter, up to 2 mm thick), in view of their better optical quality and higher light yield in the Phase I research. These measurements were carried out using 511 keV photons (^{22}Na source).

a. Timing Resolution:

Figure 15. Setup for measuring coincidence timing resolution of ceramic hafnates.

Comment [CB2]: Figure 14 is missing

Deleted: 23

Deleted: to be used to

Deleted: e

During the Phase I research, we measured the coincidence timing resolution of selected ceramic $SrHfO_3$:Ce samples at LBNL using the setup shown in **Figure 15**. This experiment involved irradiating a BaF_2 crystal and a hafnate ceramic (each coupled to a fast PMT) with 511 keV positron annihilation γ-ray pair (emitted by a ^{68}Ge source). The BaF_2-PMT detector formed a "start" channel in the timing circuit, while the $SrHfO_3$-PMT detector formed the "stop" channel. The signal from each detector was processed using two channels of a Tennelec TC-454 CFD that had been modified for use with fast (sub-ns) rise-time PMTs. The time difference between the start and stop signals was digitized with a Tennelec TC-862 TAC and a 16-bit ADC, resulting in a TDC with 7.5 ps per bin resolution. Coincidence timing data were accumulated in this manner.

Figure 16 shows a coincidence timing resolution plot acquired in this manner using an early $SrHfO_3$:Ce ceramic specimen and the timing resolution was estimated to be ~400 ps (FWHM) at room temperature, which is very encouraging. This study confirms that due to fast response and relatively high light output, excellent coincidence timing resolution can be achieved with the $SrHfO_3$:Ce ceramics.

With better quality $SrHfO_3$:Ce samples that were produced subsequently in the Phase I effort, further improvement in timing resolution of the ceramic scintillators was achieved. These timing resolution experiments were conducted at U-Penn by Dr. Karp's group in the Phase I research using a better quality $SrHfO_3$ ceramic (1 cm diameter, 2 mm length). The reference detector in this case was a thin slice (~2 mm thick, 1 cm diameter) of cerium bromide ($CeBr_3$), a new, fast scintillator being investigated at RMD (<0.1 ns risetime, 17 ns decay time). Fast PMTs (Hamamatu's R4998) were used in both timing chains and a coincidence timing distribution plot is shown in **Figure 17**. The timing resolution is estimated to be ~230 ps (FWHM), which is very encouraging. Based on prior calibration of the thin $CeBr_3$ sample, the coincidence timing resolution of two hafnate samples can be estimated to be ~320 ps (FWHM).

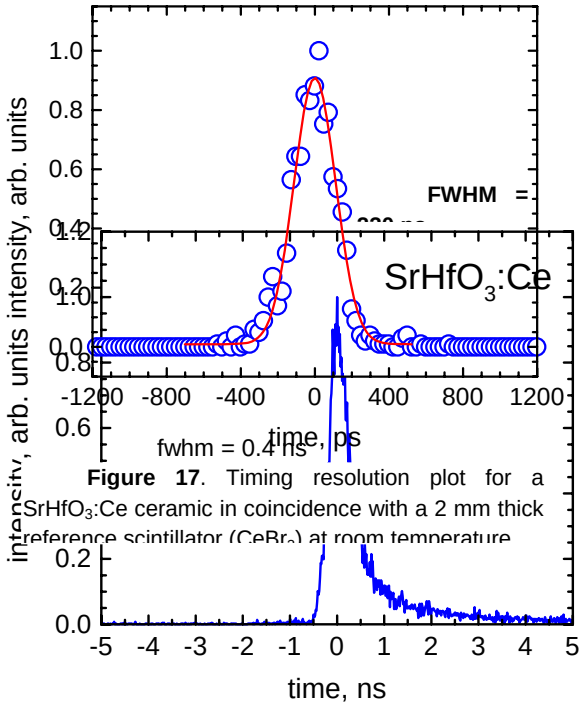

Figure 16. Timing resolution spectrum for a ceramic $SrHfO_3$:Ce-PMT detector in coincidence with a BaF_2-PMT detector upon exposure with 511 keV γ-ray

Figure 17. Timing resolution plot for a $SrHfO_3$:Ce ceramic in coincidence with a 2 mm thick reference scintillator ($CeBr_3$) at room temperature

This result confirms that $SrHfO_3$:Ce is indeed a very promising scintillator for PET. Upon optimization of these specimens in the Phase II research, we expect further improvement in their timing resolution. Ultimately, these samples should provide excellent rejection of randoms in PET and may also be promising for time-of-flight PET imaging.

b. Energy Resolution Studies

Deleted: 24

The final set of experiments performed in the Phase I research involved coupling a high quality $SrHfO_3$:Ce optical ceramic to a PMT and collecting energy spectra upon exposure to selected gamma-ray energies. In view of the intended PET application, we primarily focused on 511 keV gamma-rays. The scintillator was wrapped in Teflon tape, coupled to a PMT using optical grease and irradiated with 511 keV gamma-rays (^{22}Na source). The resulting energy spectrum, collected at room temperature, is shown in **Figure 18**. The energy resolution of 511 keV photopeak is very good, ~17% FWHM, which is very respectable for an early specimen. Proportionality of response for the ceramic $SrHfO_3$:Ce specimen was also evaluated in the Phase I research and over 60 keV to 662 keV energy range, the non-proportionality was measured to be about 7%, which is better than that for many established scintillators. For example, over the same energy range, the non-proportionality is over 20% for LSO. Since non-proportionality (as a function of energy) in light yield is one of the important reasons behind the degradation in energy resolution of established scintillators such as LSO [3], the higher proportionality for the ceramic hafnate specimens indicates that as samples with better optical quality and higher light output are produced, better energy resolution should be achievable.

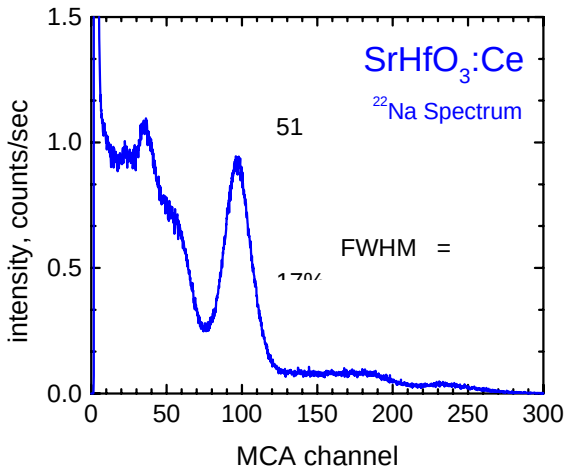

Figure 18. ^{22}Na spectrum recorded with a $SrHfO_3$ ceramic sample (1 cm diameter, 2 mm thick) in the Phase I effort

Comment [CB3]: Figure 18 is missing

The energy and timing resolution results recorded for our hafnate ceramics in Phase I research is comparable or better than those for single crystal BGO and LSO crystals, which is very encouraging. Overall, the results of our Phase I effort confirm the great potential of the hafnate ceramic scintillators for PET imaging and clearly demonstrate the feasibility of the proposed effort.

6. SUMMARY

The research in Phase I was aimed at demonstrating the feasibility of producing high performance $SrHfO_3$:Ce and $BaHfO_3$:Ce scintillators by means of ceramic technology. During the Phase I research, we ascertained the appropriate ceramic fabrication conditions to synthesize cerium-activated $SrHfO_3$ and $BaHfO_3$ and began optimization of the controlling factors. Synthesis of both powders and ceramics was accomplished. Characterization of morphological and optical properties of the ceramic $SrHfO_3$:Ce and $BaHfO_3$:Ce samples was be carried out. Investigation of scintillation properties such as light output, emission spectrum, decay time, and energy and timing resolution was also conducted. Overall, our results confirmed that ceramic hafnates provide fast response, excellent timing resolution as well as high light output and energy resolution. These results in combination with high gamma-ray stopping efficiency of the selected hafnates as well as overall potential of the ceramic processing approach confirm that

these new scintillators are very attractive for PET imaging. Further optimization of these ceramic scintillators will be carried out in the Phase II project.

---

i (Issler)
ii (Bollinger)